

Original

β -lapachone nanostructured lipid carriers: repolarization of tumor-associated macrophages for osteosarcoma therapy

Rebeca Martínez-Borrajó, Arturo Alejandro Lorenzo-Lorenzo, Mariana Landin, Patricia Díaz-Rodríguez

Department of Pharmacology. Pharmacy and Pharmaceutical Technology. Grupo I+D Farma (GI-1645). Faculty of Pharmacy. Instituto de Investigación Sanitaria de Santiago de Compostela (IDIS). Instituto de Materiais da Universidade de Santiago de Compostela (iMATUS). Universidade de Santiago de Compostela. Santiago de Compostela, A Coruña. Spain

Abstract

Osteosarcoma (OS) is the most common primary malignant bone tumor. Tumor-associated macrophages (TAMs) represent up to 50 % of the cells in the tumor and play a significant role in tumor metastasis and tumoral immunosuppression. The modification of TAMs phenotype has been identified as suitable for controlling tumor progression. Nanoparticles are versatile drug delivery systems that allow enhanced drug tumor accumulation through passive and active targeting. Among NPs, nanostructured lipid carriers (NLCs) possess a unique imperfect matrix structure with increased drug loading capacity of highly hydrophobic drugs. β -Lapachone (β -Lap) is a natural naphthoquinone with anti-tumor activity against various cancer cells. The aim of this work is to design and optimize a NLCs formulation loaded with β -Lapachone to be specifically internalized by TAMs for OS treatment. This approach will use hybrid artificial intelligence tools to functionalize the NLCs with the CD206 ligand mannose. To optimize NLCs preparation, various liquid and solid lipids were tested for drug solubility. AI tools were employed to design NLCs with desired properties, resulting in formulations with particle sizes < 100 nm and stable physicochemical properties. Mannose functionalization enhanced macrophage internalization of the NLCs. Moreover, *in vitro* studies demonstrated these NLCs, particularly the mannose-functionalized formulation, induced a further pro-inflammatory M1-like polarization in TAMs, evidenced by increased TNF- α and IL-6 secretion. This TAMs polarization strategy, combined with the localized delivery of β -Lap, offers a promising approach for OS therapy.

Keywords:

Osteosarcoma.
Tumor-associated
macrophages.
Targeted drug
delivery. Tumor
environment
modulation.

Received: 04/21/2025 • Accepted: 07/23/2025

Patricia Díaz-Rodríguez (patricia.diaz.rodriguez@usc.es) and Mariana Landin (m.landin@usc.es) are both the corresponding authors of this article.

Acknowledgements: This research was supported by the "Becas FEIOMM investigación 2021" (2021-PO060). Work partially financed by Xunta de Galicia [ED431C 2024/09], FEDER and Xunta de Galicia-GPC (IN607B 2024/10).

Conflict of interest: The authors declare no conflict of interest.

Artificial intelligence: The authors declare not to have used artificial intelligence (AI) or any AI-assisted technologies in the elaboration of the article.

Martínez-Borrajó R, Lorenzo-Lorenzo AA, Landin M, Díaz-Rodríguez P. β -lapachone nanostructured lipid carriers: repolarization of tumor-associated macrophages for osteosarcoma therapy. Rev Osteoporos Metab Miner 2025;17(3):117-127

DOI: 10.20960/RevOsteoporosMetabMiner.00082

Correspondence:

Patricia Díaz-Rodríguez. Faculty of Pharmacy.
Instituto de Investigación Sanitaria de Santiago
de Compostela (IDIS). Hospital Clínico, edificio
D, 1.ª planta. Travesía da Choupana, s/n. 15706
Santiago de Compostela, A Coruña. Spain
e-mail: patricia.diaz.rodriguez@usc.es

INTRODUCTION

Osteosarcoma (OS) is recognized as the most prevalent bone primary malignant tumor. It shows an incidence peak in the 2nd decade of life associated to an enhanced activity of the metaphyseal plates and affects more than 9 teenagers per million in the range of 15-19 years-old (1). The most prevalent locations for OS are the femur, tibia, and proximal humerus, particularly around the knee (2,3). In approximately 75 % of cases, the tumor is located within the metaphysis of long bones, where it grows rapidly, extending to the bone periphery (4). The typical clinical signs of OS include localized pain followed by swelling and restricted joint movement. Although rare, a pathological fracture can also occur at the site of the disease (5). OS can be categorized into several types based on the predominant produced matrix (chondroblastic, fibroblastic or osteoblastic) or the malignant grade, which aids in assessing the tumor's metastatic potential (4,6). Regarding its physiopathological origin, the main cause is believed to be the accumulation of genetic mutations in mesenchymal stem cells (MSCs) during their differentiation into osteoblasts (7,8). Surgery and radiation therapy and chemotherapy remain the primary treatment options and are frequently combined for metastatic tumors (9). However, conventional chemotherapy presents several limitations such as drug resistance and side effects (10).

The primary histopathological feature of OS is the excessive production of osteoid tissue, the unmineralized organic component of the bone matrix formed before tissue maturation (11). This matrix is produced by malignant cells of the mesenchymal lineage comprising MSCs, osteoprogenitor cells and osteoblasts (11-13). Furthermore, bone mineral metabolism is also altered and is thought to play a role in several aspects of tumor progression (14,15). OS presents an osteoclastic stimulatory environment increasing the activity of these bone-resorbing cells. This effect is mediated by the secretion of soluble factors. Simultaneously, the induced osteolysis promoted the release of tumor growth inductors, creating a cycle of bone destruction and tumor formation (12,14). The final outcome is the establishment of a metabolic state which increases the production of immature, weaker, and disorganized bone matrix together with the hyperactivity of osteoblasts and osteoclasts (12,14,15).

Additionally, tumor-associated macrophages (TAM) and myeloid-derived suppressor cells (MDSCs) amplify the alterations in bone homeostasis (14). The tumoral microenvironment (TME) formed by tumoral cells, immune cells, stromal cells, extracellular matrix and soluble mediators plays a key role in tumor progression and chemotherapy efficacy (16). In this scenario, immune cells can either facilitate or inhibit tumor growth (17). Specifically, tumor-associated macrophages (TAMs) constitute a significant portion

of OS mass, representing up to 50 % of the cells (18). They perform essential functions related to bone formation and osteoblast differentiation and have been identified as main players in tumor metastasis and tumoral immunosuppression (19-21). Macrophages can depict opposing phenotypes, with different functions: the inflammatory phenotype or classical (M1) and the anti-inflammatory or alternative phenotype (M2). Overall, M1-TAMs are associated with tumor inhibition and M2-TAMs with a neoangiogenic effect and secrete cytokines such as IL-1 β leading to tumor progression and metastasis (22-24). Given the role of TAMs in controlling tumor progression, multiple strategies based on either avoiding their M2 polarization or suppressing the M2-TAMs profile inducing an M1-TAMs have been proposed to control OS (21,25). Clinical trials have shown that the addition of mifamurtide to the standard chemotherapy treatment, results in an increase in 6-year survival rate in OS patients (26). The mechanism of action of this therapeutic molecule is thought to be associated with its ability to *in vitro* switch M2-TAMs towards and intermediate M1/M2-TAMs, proving that polarization to M1-TAMs was key for controlling tumor progression (27). The development of drug delivery systems targeting TAMs could enable the efficient control of macrophage polarization and, therefore, improve the treatment of OS. This approach seeks to selectively control the macrophage population towards a pro-inflammatory response avoiding undesired side effects. Nanoparticles (NPs) are versatile drug delivery systems with improved pharmacokinetic profiles vs free therapeutic molecules. These systems allow for enhanced circulation time and accumulation within the tumor through passive and active targeting (28). In this case, the surface can be modified to incorporate specific moieties with affinity for the bone extracellular matrix or for cell surface receptors. Several targeted NPs loaded with chemotherapy drugs have been developed for OS management including liposomes, polymeric NPs, mesoporous silica nanocarriers, manganese dioxide NPs and iron oxide NPs (29,30). However, these strategies are mainly focused on controlling proliferative cells and, as far as we know, no TAMs targeted NPs have been reported for OS management.

β -Lapachone (3,4-dihydro-2,2-dimethyl-2H-naphtho[1,2-b]pyran-5,6-dione) (β -Lap) is a natural naphthoquinone extracted from the lapacho tree. It exhibits anti-tumor activity against various cancer cells, including breast cancer, leukemia, prostate cancer, bladder cancer, lung cancer, hepatoma, pancreatic cancer, and OS. β -Lap induces a redox cycle mediated by NAD(P)H:quinone oxidoreductase 1 (NQO1) (31,32). During this process, β -Lap is reduced to an unstable semiquinone that undergoes a two-step oxidation process, returning to its stable form and perpetuating a futile redox cycle. The generated redox cycle disrupts intracellular reactive oxygen species (ROS) balance, leading to cell death through apoptosis and necrosis (necroapoptosis).

This mechanism of action confers drug specificity towards hypoxic tumor regions usually highly infiltrated in TAMs (33). Moreover, an upregulated expression of this anti-oxidant enzyme has been reported in anti-inflammatory M2 macrophages (34). Moreover, some studies have shown that ROS play a key role in macrophage differentiation. Specifically, ROS in tumoral environment activates macrophages to a M1 pro-inflammatory and antitumoral state (35).

Despite β -Lap has the potential to modulate tumor microenvironment in OS avoiding tumor growth and metastasis, its poor water-solubility hinders bioavailability (36). Moreover, while it exhibits preferential activity in cells overexpressing NQO1, improving the drug cellular specificity is necessary to avoid undesired side effects. In this scenario, the development of β -Lap loaded TAMs targeted drug delivery systems will allow to specifically modulate the phenotype of TAMs towards a pro-inflammatory and anti-tumoral profile. Among nanoparticulated drug delivery systems, nanostructured lipid carriers (NLCs) possess a unique imperfect matrix structure with enhanced properties, such as increased drug loading capacity of highly hydrophobic drugs, greater stability during storage, and controlled drug release. Moreover, their surface can be modified by incorporating glycoligands such as mannose, fucose, or glucose for targeting specific cell membrane receptors on macrophages. Therefore, NLCs could be adequate to fine-tune nanocarriers for macrophage polarization control (37-41).

The design of drug delivery systems such as NLCs, is a complex process with several variables involved. Computational techniques have been used to model results, make predictions, and even optimize different formulations (42-44). Artificial neural networks (ANNs), an artificial intelligence (AI) technique that mimics the functioning of the human brain, can be integrated with other AI tools, such as Fuzzy Logic (FL) or Genetic Algorithms (GAs) to create hybrid systems capable of modelling complex manufacturing processes. These computational techniques have been used as effective tools for optimizing the development of NLCs. By incorporating variables such as composition and operation conditions, these techniques enable refined control and prediction of particle size, polydispersity index, zeta potential, and drug loading capacity, ensuring the development of robust and reproducible designs (45,46).

The aim of this work is to design and optimize a NLCs formulation loaded with β -Lapachone to be specifically internalized by TAMs for OS treatment. This approach will be performed by using hybrid artificial intelligence tools (AI tools) functionalizing the NLCs with the CD206 ligand mannose. The developed system would induce immune cellular response (M1-TAMs polarization), leading to a decrease in tumor growth by dual cellular and chemical action.

MATERIALS AND METHODS

MATERIALS

β -Lapachone (β -Lap) was kindly donated by the Pernambuco State Pharmaceutical Laboratory, LAFEPE (Recife, Brazil). Miglyol[®], Transcutol[®] CG, Labrasol[®] ALF, Labrasol[®] Lipophile WL, Transcutol[®] HP, selected as liquid lipids (LL), were kindly provided by Gattefossé (France). Oleic Acid was also selected as LL and it was acquired from Merck (Portugal). Compritol[®] 888 ATO, Precirol[®] ATO and Glycerol Tristearate were selected as solid lipids (SL) and kindly gifted by Gattefossé (France). Polysorbate 80 (Tween[®] 80), purchased from Sigma Aldrich (Germany), and lecithin (Epikuron[®] 145 V), donated by Cargill (USA), were used as surfactants. Milli-Q[®] water (Milli-Q[®] plus, Millipore Iberica, Spain) was used throughout all the experiments. For the functionalization process, stearylamine and D-(+)-Mannose were acquired from Sigma-Aldrich (USA). The acetate buffer was prepared using acetic acid 0.2 M from Sigma Aldrich (USA) and sodium acetate 0.2 M from Scharlab (Spain).

SELECTION OF NLCs COMPONENTS

β -Lapachone solubility in liquid lipids

The solubility of β -Lap in different LL was assessed following a previously described procedure (45). To this end, 200 mg of β -Lap was mixed with 1 mL of each LL. The mixture was stirred at 300 rpm for 48 hours. Then samples were centrifuged at 12,000 rpm and 20 °C for 30 min and properly diluted in acetonitrile. The amount of solubilized β -Lap was quantified by UV-Visible spectrophotometry using an Agilent Technologies UV-VIS 8453 spectrophotometer (USA) at 257 nm, employing a previously validated calibration curve. Solubility studies were conducted in triplicate.

β -Lapachone solubility in solid lipids

The solubility of β -Lap in different LL was also assessed following a previously described procedure (45). To this end, 200 mg of each SL was heated in a water bath at 80 °C (5 °C above its melting point). Once the SL was melted, β -Lap was added in 5 mg increments until a precipitate appeared, indicating the presence of non-solubilized β -Lap.

Miscibility studies of liquid lipids and solid lipids

LL and SL were mixed in various ratios (50:50, 25:75, 75:25). The mixtures were heated in a water bath at 80 °C with continuous stirring for 5 minutes, phase separation was evaluated as indicative of immiscibility.

Experimental design

Dataform® v3.1 software (Intelligensys Ltd., UK) was used to establish a reduced and balanced experimental design for three variables: LL:SL ratio, concentration of Tween® 80 (% v/v) in the aqueous phase, and percentage of lecithin relative to the total lipid phase. The obtained experimental design conditions are shown in table I.

Formulation	LL:SL ratio	Tween® 80 (% v/v)	Lecithin (% w/v)
1	30:70	2.00	2.0
2	50:50	0.50	1.5
3	10:90	1.25	1.0
4	30:70	1.25	1.5
5	50:50	2.00	1.0
6	10:90	0.50	2.0
7	50:50	2.00	2.0
8	10:90	1.25	1.5
9	30:70	0.50	1.0

NANOSTRUCTURED LIPID CARRIERS FORMULATION

NLCs were prepared using a high-shear hot homogenization method similarly to previously described (46). Based on the solubility of β -Lap in the different LL and SL lipids, Compritol® 888 ATO (COMP) and Transcutol® HP (THP) were selected as lipid components, while Tween® 80 and lecithin were used as surfactants. A lipid blend of 300 mg was prepared containing the LL and SL in the proportions indicated in table I. The drug was incorporated into this phase on the basis of its LL solubility. Separately, an aqueous phase was prepared by adding lecithin to 10 mL of a Tween® 80 solution in milli-Q water as specified in table I. Then, both phases were heated in a water bath at 80 °C for 5 minutes, and the aqueous phase was then added to the lipid blend and homogenized using an Ultra-Turrax T25 (IKA Labortechnik, Germany) for 10 minutes at 14,800 rpm. Finally, the resulting NLCs dispersion was cooled in an ice-water bath for two minutes with gentle stirring. The dispersions were stored at 4 °C until characterization (41,45,47).

NANOSTRUCTURED LIPID CARRIER CHARACTERIZATION

NLCs dispersions were characterized in terms of particle size, polydispersity index (Pdl) and surface charge (ZP) using a Zetasizer Nano-ZS (Malvern Instruments, UK). Samples were diluted in milli-Q water (1:10), and

polystyrene cuvettes were used for particle size and Pdl measurements (DTS0012, Malvern Instruments, UK). Measurements were conducted at 25 ± 1 °C, and NLCs were characterized 15 minutes and 14 days after preparation. Surface charge was determined by measuring particle mobility in an electric field to calculate the Zeta potential (ZP). Samples were also diluted in milli-Q water (1:10), and measurements were performed using a Malvern DTS 1070 cuvette 15 minutes and 14 days after NLC preparation.

NLCs dispersions were also characterized in terms of drug loading (DL) and encapsulation efficiency (EE). To this end, NLCs were purified using cellulose membranes (MWCO: 3.5 kDa from Spectra/Por®). Afterwards, the purified dispersion was dissolved in acetonitrile (1:2 dilution) to release the encapsulated drug and centrifuged at 12,000 rpm, 4 °C for 30 minutes. The encapsulated drug was quantified spectrophotometrically using a plate reader (FLUOstar Omega, BMG Labtech, Germany) at 280 nm. The same procedure was performed for non-purified NLCs to determine the total drug amount (free drug + encapsulated drug). The DL and EE were calculated using equation 1 and equation 2, respectively,

$DL (\%) = \left[\frac{\text{Encapsulated drug (mg)}}{\text{Weight of NLCs (mg)}} \right] \times 100$	(Eq. 1)
$EE (\%) = \left[\frac{\text{Encapsulated drug (mg)}}{\text{Total drug (mg)}} \right] \times 100$	(Eq. 2)

NANOSTRUCTURED LIPID CARRIER FORMULATION MODELLING USING ARTIFICIAL INTELLIGENCE TOOLS

INForm® v5.01 (Intelligensys Ltd, UK) is a commercial software that integrates ANN, and GAs, specifically designed for modelling and optimizing pharmaceutical formulations such as NLCs. This software was used to model the generated experimental database (Table II). Three variables were included as inputs: LL/SL ratio, the percentage of Tween® 80 in the aqueous phase, and the percentage of lecithin relative to the total lipid phase. Four variables were included as outputs: particle size, Pdl and ZP after 14 days of storage and DL. The modelling was carried out using the default software parameters.

Composition conditions were selected to produce an optimal formulation based on the following requirements: particle size and Pdl with the lowest possible values, ZP with the most negative values at 14 days, and maximum DL. The optimal formulation was experimentally prepared. Unloaded (NLC) and drug-loaded formulations (NLC- β -Lap) were prepared to validate the generated model.

NANOSTRUCTURED LIPID CARRIERS SURFACE FUNCTIONALIZATION

Optimal formulations (NLC- β -Lap) were functionalized with mannose (NLC- β -Lap-MAN). To achieve this, stearylamine (2 % w/w) (relative to the total lipid phase) was added to the lipid blend, and the formulation was prepared as described in section 2.4. The formulation was then incubated with a 50 mM D-(+)-mannose solution prepared in acetate buffer at pH 4, and stirred vigorously for 48 hours, similarly to previously described (45,48,49). The formulation was subsequently dialyzed using a cellulose membrane (MWCO: 3.5 kDa) against milli-Q water with agitation for 30 minutes to remove potential impurities and unattached mannose.

IN VITRO CELL STUDIES

In vitro cell studies were conducted in human monocytes derived from acute lymphocytic leukaemia (THP-1) acquired from ATCC (TIB-202) (USA). THP-1 cells were cultured in RPMI 1640 media supplemented with foetal bovine serum (FBS) (10 %), penicillin/streptomycin (1 %) and 2-mercaptoethanol 0.05 mM. Before studies, cells at a density of 2×10^5 cells/mL were stimulated with 200 nM of phorbol 12-myristate 13-acetate (PMA) acquired from Sigma-Aldrich (USA) in complete RPMI 1640 media for 48 hours to induce their differentiation to macrophages. Finally, cell monolayers were washed with Dulbecco's phosphate-buffered saline (DPBS), and incubated with complete RPMI 1640 media, allowing them to set for 24 h at 37 °C and 5 % of CO₂ before seeding.

Cell viability studies

Cells were seeded in 96-well plates (2×10^4 cells/well). After 24 hours, the optimized formulations (NLC, NLC- β -Lap, and NLC- β -Lap-MAN) were added at a final 300 μ g/mL (solid mass per volume) concentration and incubated for 24 hours. As control, cells treated with an equivalent amount of milli-Q water were used. After this time, cell viability was evaluated using the "Cell Proliferation Reagent WST-1" kit from Roche Molecular Biochemicals (Germany) following the manufacturer's instructions. A phenol red-free medium from Gibco (USA) was used, and the WST-1 reagent was applied in darkness. The reagent was also added to wells without cells to serve as absorbance blanks. The plate was incubated with the reagent for 1 hour at 37 °C and then shaken for 1 minute. The absorbance at 450 nm was determined on a plate reader (Bio-Rad 680, Barcelona, Spain). Cell viability was calculated using equation 3.

$$\text{Cell viability (\%)} = \left[\frac{\text{Sample absorbance-Blk}}{\text{Control absorbance-Blk}} \right] \times 100 \quad (\text{Eq. 3})$$

Cell internalization studies

Cells were seeded in 96-well plates (2×10^4 cells/well). After 24 hours, fluorescently labelled formulations (NLC- β -Lap and NLC- β -Lap-MAN) prepared by adding coumarine-6 (4 μ g/mL) to the lipid blend during the NLC formulation were added at a final concentration of 300 μ g/mL (solid mass per volume) and incubated for 2 hours to quantify their internalization using a fluorometric method. An initial fluorescence measurement was obtained with a plate reader (FLUOstar Omega, BMG Labtech, Germany) at excitation and emission wavelengths of 485 nm and 520 nm, respectively. After 2 hours, 3 washes were performed with 20 mM glycine solution from Fluka BioChemika (Switzerland) in DPBS at pH 7.4. Afterwards, 100 μ L/well of Triton X-100 (1 %) from Merck (Portugal) was added to induce cell lysis, allowing the internalized formulations to be released. Fluorescence measurements were then taken post-lysis in the same conditions. The percentage of NPs internalization was determined using equation 4.

$$\text{Cell internalization (\%)} = \left[\frac{\text{Post-lysis fluorescence}}{\text{Initial fluorescence}} \right] \times 100 \quad (\text{Eq. 4})$$

Evaluation of the tumor-associated macrophages profile modification

The capacity of the developed formulations to modulate TAMs phenotype was tested using THP-1 macrophages. Cells were seeded in 96-well plates (2×10^4 cells/well) and allowed to attach for 18 h. Monolayers were then stimulated with lipopolysaccharide (LPS) (100 ng/mL) for 24 h to obtain activated macrophages serving as TAMs models. Following stimulation, cells were then treated with the developed formulations (NLC- β -Lap, and NLC- β -Lap-MAN) at a final concentration of 300 μ g/mL (solid mass per volume). Stimulated but untreated cells were used as controls. After 24 hours, cell culture supernatants were collected, and the secreted concentrations of various cytokines and matrix degradative enzymes involved in tumor invasion, metastasis and OS osteolysis (TNF- α , IL-6, IL-8, IL-1RA, and IL-13) were determined using a magnetic bead-based multiplex assay (R&D systems, USA) and according to the manufacturer's instructions for use.

STATISTICAL ANALYSIS

The obtained data was analysed with GraphPad Prism 8 software through one-way analysis of variance (ANOVA) followed by post hoc Tukey's Multiple Comparison Test. Results are expressed as mean \pm SD. Statistically significant differences were set at $p < 0.05$.

RESULTS

NANOSTRUCTURED LIPID CARRIERS COMPONENTS SELECTION

Although β -Lap is highly insoluble in water, its lipid solubility was unknown. This study evaluated the β -Lap solubility across different liquid lipids (Fig. 1), revealing statistically significant variation. Transcutol® CG (TCG), Labrasol® ALF, and Transcutol® HP exhibited the highest β -Lap solubilization capacity, while Labrasol® Lipophile WL showed the lowest (Fig. 1). Consequently, Transcutol® CG (TCG), Labrasol® ALF, and Transcutol® HP were selected for further development.

Solubility tests in solid lipids revealed β -Lap was less soluble in Precirol® ATO than in the other SL. Therefore, Precirol® ATO was excluded. Additionally, glyceryl tristearate was excluded due to its immiscibility with the selected LL. On the other hand, Compritol® 888

ATO (COMP) mixed with the LL with high β -Lap solubility (Transcutol® CG, Labrasol® ALF and Transcutol® HP) showed no phase separation. Preliminary blank NLC formulations with a 50:50 LL-to-SL ratio, Tween 2 % v/v relative to the aqueous phase, and lecithin 1 % w/v relative to the lipid phase were prepared to determine the most suitable LL/SL combination (data not shown). Based on these results, Transcutol® HP was selected, as it produced NLCs with the smallest and most homogeneous particle size distribution, appropriate ZP values and good stability after 14 days of storage at 4 °C.

NANOSTRUCTURED LIPID CARRIERS CHARACTERIZATION AND OPTIMIZATION

The formulations shown in table I were prepared and characterized in terms of particle EE and DL 15 minutes post-preparation, and again in terms of size, Pdl and ZP after 14 days of storage at 4 °C (Table II).

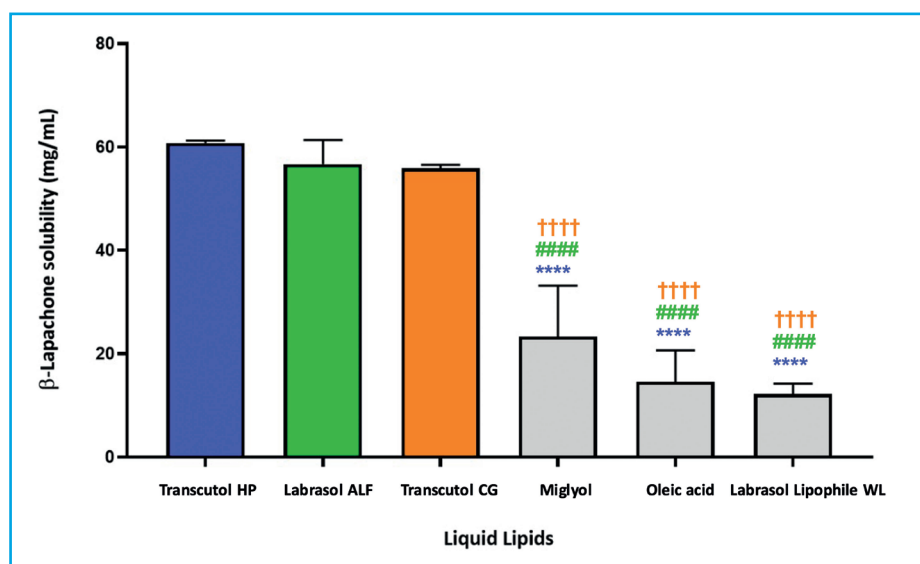


Figure 1. β -Lapachone solubility across different liquid lipids. Values are expressed as mean \pm SD ($n = 3$). (****) $p < 0.0001$ vs. Transcutol® HP; (####) $p < 0.0001$ vs. Labrasol® ALF; and (††††) $p < 0.0001$ vs. Transcutol® CG.

Table II. NLCs characteristics 15 minutes and 14 days after their preparation and storage at 4 °C

NLCs	NLCs characteristics ($t = 15$ min)					NLCs characteristics ($t = 14$ days)		
	Particle size (nm)	Pdl	ZP (mV)	EE (%)	DL (%)	Particle size (nm)	Pdl	ZP (mV)
1	90.3 \pm 37.9	0.29 \pm 0.02	-13.0 \pm 6.2	15.0 \pm 2.5	0.4 \pm 0.2	88.7 \pm 39.8	0.24 \pm 0.02	-12.2 \pm 7.7
2	147.2 \pm 76.2	0.34 \pm 0.03	-18.9 \pm 6.1	14.1 \pm 16.8	0.4 \pm 1.3	143.3 \pm 85.7	0.36 \pm 0.01	-19.2 \pm 7.4
3	157.7 \pm 77.0	0.28 \pm 0.01	-15.7 \pm 5.0	6.1 \pm 0.2	0.1 \pm 0.0	156.8 \pm 71.6	0.29 \pm 0.02	-16.9 \pm 5.9
4	104.9 \pm 38.9	0.26 \pm 0.06	-18.5 \pm 6.7	7.5 \pm 0.0	0.2 \pm 0.1	102.6 \pm 38.4	0.26 \pm 0.04	-15.4 \pm 6.1
5	122.9 \pm 52.7	0.23 \pm 0.01	-11.5 \pm 6.7	15.3 \pm 4.0	0.7 \pm 0.8	124.2 \pm 49.1	0.23 \pm 0.02	-11.1 \pm 6.2
6	329.9 \pm 193.4	0.32 \pm 0.03	-18.6 \pm 6.6	4.4 \pm 1.4	0.1 \pm 0.0	316.1 \pm 195.1	0.34 \pm 0.06	-18.0 \pm 4.8
7	97.6 \pm 38.4	0.27 \pm 0.02	-14.9 \pm 5.2	16.9 \pm 9.6	0.9 \pm 1.4	98.5 \pm 38.4	0.26 \pm 0.01	-10.0 \pm 5.1
8	149.5 \pm 67.4	0.31 \pm 0.02	-15.9 \pm 6.3	5.7 \pm 0.3	0.1 \pm 0.1	164.5 \pm 96.9	0.31 \pm 0.01	-15.8 \pm 4.7
9	261.6 \pm 151.7	0.38 \pm 0.05	-18.1 \pm 5.8	7.4 \pm 6.2	0.2 \pm 0.4	251.5 \pm 163.2	0.36 \pm 0.02	-18.4 \pm 5.9

NANOSTRUCTURED LIPID CARRIERS MODELLING USING ARTIFICIAL INTELLIGENCE TOOLS AND FUNCTIONALIZATION

INForm® v5.01 software was employed to optimize the composition for β-Lap-encapsulating NLCs (NLC-β-Lap). The software selected the formulation that meet all pre-defined criteria, specifically, minimizing particle size and Pdl after 14 days at 4 °C while maintaining a negative ZP for stability. The optimal formulation consisted of a 50:50 LL:SL ratio, 1.12 % (v/v) of Tween 80 and 1.17 % of lecithin (w/v). Predicted and experimental values for this formulation are shown in table III.

Table III illustrates the model's accurate prediction of particle size, Pdl and ZP, with experimental values closely aligned with predictions. The stability of the formulations over 14 days was confirmed by the experimental Pdl and ZP values. However, the model overestimated the drug loading capacity (DL) in agreement with former studies, the limited number of loaded formulations within the database limits the accuracy of the model. Consequently, while the model provides reliable initial estimations for particle size, Pdl and ZP, further adjustments and experimental validations are necessary to improve its precision regarding DL.

In agreement with previous works (41,45,49), the mannose functionalization of NLCs yielded a shift in the

surface charge to positive ZP values for both, blank (NLC) (+ 32.6 ± 5.9 mV) and β-Lap loaded formulations (NLC-β-Lap) (+ 24.1 ± 6.4 mV).

IN VITRO CELL STUDIES

Macrophages were treated for 24 h with NLC, NLC-β-Lap, and NLC-β-Lap-MAN at a final concentration of 300 µg/mL. Untreated cells were used as control. Cell viability is shown in figure 2A. Statistical analysis revealed no significant differences in cell viability among the formulations. Cell viability values were close to 100 % for all formulations, demonstrating high cytocompatibility, regardless of β-Lap incorporation. As expected, blank formulations (NLC) had no adverse effect on cell viability due to the GRAS (Generally Recognized as Safe) status of their excipients.

Since cell viability was consistent across all formulations, subsequent experiments were focused on drug-loaded formulations (NLC-β-Lap and NLC-β-Lap-MAN) (300 µg/mL). Internalization assays (Fig. 2B) demonstrated statistical significantly higher uptake for mannose-functionalized formulations (NLC-β-Lap-MAN) vs non-functionalized ones (NLC-β-Lap), confirming successful mannose coating and enhanced macrophages internalization, which is consistent with previous works (48,49).

Table III. NLCs characteristics predicted by the INForm® software and the experimental results

NLC predicted characteristics		NLC characteristics after 15 minutes		NLC characteristics after 14 days of storage	
Characteristics	Predicted values	Experimental values (NLC)	Experimental values (NLC-β-Lap)	Experimental values (NLC)	Experimental values (NLC-β-Lap)
Size (nm)-day 14	116.6	85.4 ± 33.4	89.2 ± 42.9	76.0 ± 25.3	77.8 ± 28.4
Pdl-day 14	0.28	0.28 ± 0.02	0.25 ± 0.02	0.28 ± 0.03	0.22 ± 0.03
ZP (mV)-day 14	-18.5	-18.1 ± 6.6	-14.4 ± 7.9	-14.8 ± 5.3	-14.2 ± 6.0
DL (%) -15 min	0.5	-	0.01 ± 0.00	-	0.14 ± 0.02

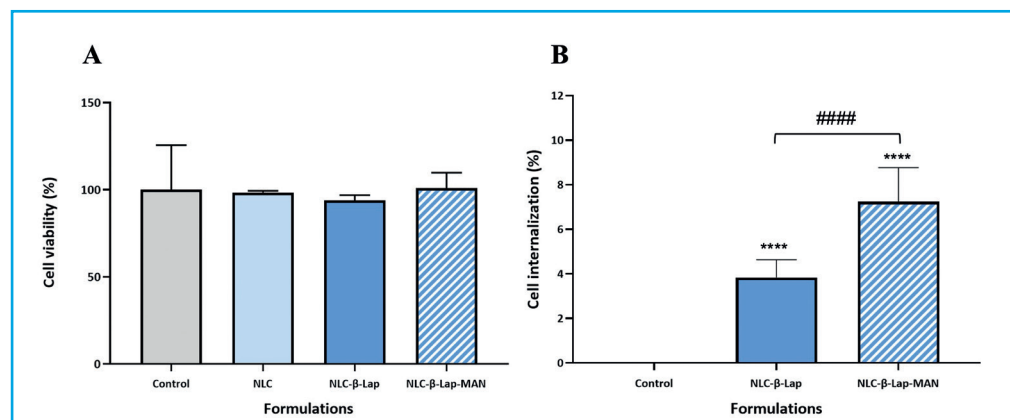


Figure 2. A. THP-1 cell viability after 24 h treatment with formulations (300 µg/mL). B. THP-1 internalization after 24 h treatment with formulations (300 µg/mL). Untreated cells were used as a control. Values: mean ± SD (n = 6). (****) $p < 0.0001$ vs. control; (####) $p < 0.0001$ across samples.

The impact of NLC- β -Lap, and NLC- β -Lap-MAN (300 μ g/mL) on macrophage phenotypes was assessed by quantifying pro- and anti-inflammatory mediators' secretion from stimulated macrophages (TAMs) (Fig. 3).

The analysis of cytokine profiles (Fig. 3) revealed that both, NLC- β -Lap and NLC- β -Lap-MAN treatments significantly increased TNF- α and IL-6 expression vs LPS stimulated TAMs controls. No significant differences in those parameters were observed between NLCs treatments. Although IL-8 is well known to contribute to TAMs polarization toward an M2 phenotype, no significant differences were observed after treatment with the developed systems. In addition, NLC- β -Lap significantly altered the secretion of the anti-inflammatory cytokine IL-1RA while treatment with NLC- β -Lap-MAN increased the secretion of IL-13.

DISCUSSION

Osteosarcoma (OS) is the most prevalent bone primary malignant tumor where the immune system is intricately involved. Immune cells can either facilitate or inhibit tumor growth (17). Although, currently, chemotherapy is the first-line therapy, it presents several limitations such as drug resistance and associated side effects (10).

Macrophages present a high potential for immunomodulation as they can acquire opposing phenotypes (M1-TAMs or M2-TAMs), with different functions, in-

cluding bone formation, bone regeneration, and bone homeostasis (50,51). Moreover, β -Lap, a natural naphthoquinone, exhibits anti-tumoral activity against different types of cancer including OS and has demonstrated the ability to modulate intracellular ROS levels and macrophage responses (31-33).

Modulating TAMs profiles with β -Lap treatment may induce a pro-inflammatory phenotype, creating an anti-tumor environment and inhibiting tumorigenic cell proliferation (35). Therefore, β -Lap was encapsulated in nanostructured lipid carriers. To optimize NLCs preparation, various liquid and solid lipids were tested for drug solubility. Based on the solubility studies Transcutol® HP and Compritol® 888 ATO (COMP) were selected (Fig. 1). AI tools (ANN+GAs) were used to establish the optimal NLCs composition of the NLCs based on a previously generated database. The resulting models effectively predicted the nanoparticles physicochemical properties. The developed NLC and NLC- β -Lap formulations exhibited particle sizes < 100 nm and uniform size distributions (Pdl < 0.3). Moreover, moderate negative zeta potential (ZP < -15 mV) values, indicative of colloidal stability, were achieved (47). Additionally, no significant differences were observed between the freshly prepared formulations and those stored at 4 °C for 14 days, confirming the absence of aggregation during storage, and therefore, their stability (45). The INForm® v5.01 model accurately predicted particle size, Pdl, and zeta potential but overestimated the loading capacity of the systems. Despite the high solubility of β -lapachone in the selected lipids, low DL and EE values were obtained. Despite the limited loading capacity of the developed NLC, the systems exhibited therapeutic effects due to the high potency of

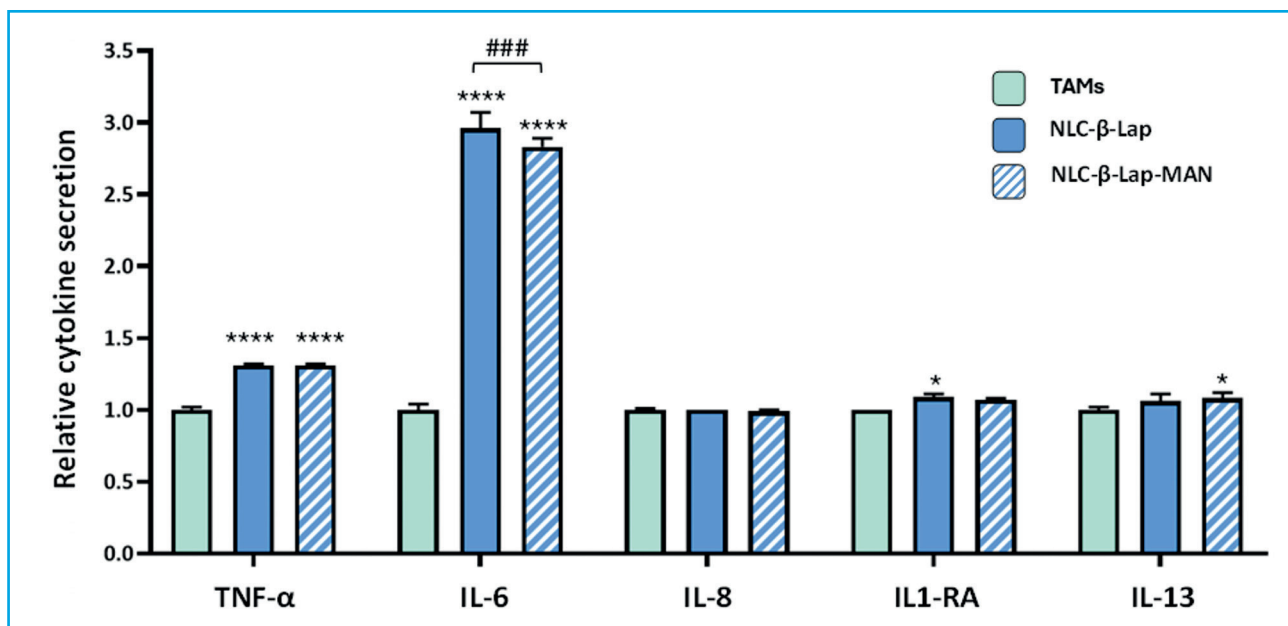


Figure 3. Relative pro-inflammatory (TNF- α , IL-6, IL-8) and anti-inflammatory (IL1-RA, IL-13) cytokines release from TAMs (100 ng/mL) 24 hours post-treatment with NLC- β -Lap and NLC- β -Lap-MAN formulations relative to untreated LPS - stimulated cells. Values: mean \pm SD ($n = 3$). (****) $p < 0.0001$ vs. TAMs; (*) $p < 0.05$ vs. TAMs; and (###) $p < 0.001$ across samples.

the drug. β -Lap is active at low concentrations showing IC50 values in tumor cells between 0.06 μ M and 48.94 μ M (52,53). The assayed NLCs were able to obtain a drug concentration of 649 μ M, that is, between 10,816 and 13.26-fold higher than the required therapeutic concentration. Strategies for enhancing drug encapsulation efficiency could include the use of a blend of different liquid lipids and solid lipids instead of selecting single LL and SL (54). Moreover, the model's capacity to predict the drug loading is restricted by the highly reduced sample number, which is an inherent constraint of the reduced experimental design (45).

Shifting macrophage polarization towards a pro-inflammatory phenotype (M1-TAMs) has the potential to decrease OS tumor growth by cellular strategies (21,25). Macrophages present recognition factors, including mannose receptors, that mediate the uptake and internalization of compounds through receptor-mediated endocytosis (55,56). To exploit this mechanism, the developed NLCs were coated with the monosaccharide mannose.

Mannose functionalization required incorporation of stearylamine (SA), which contains free amino groups that facilitate Schiff base formation ($\text{-N} = \text{CH}^-$) with the aldehyde group of mannose (57). This modification resulted in a shift from negative to positive zeta potential values. Despite mannose inherent negative charge, the excess of unreacted amino groups on the nanoparticle surface led to the observed ZP shift in both blank and β -Lap loaded formulations in agreement with previous works (41,45,49).

All formulations show cell viability values close to 100 %, indicating the high cytocompatibility of the developed formulations. Statistical analysis revealed no significant differences in cell viability among the formulations, concluding this type of NLCs does not negatively affect cell viability.

Internalization assays demonstrated mannose-functionalized NLC- β -Lap-MAN formulations exhibited nearly twice the cell uptake vs non-functionalized formulations (NLC- β -Lap). These results confirm the successful mannose coating and enhanced macrophage internalization after functionalization.

In agreement with these findings Vieira et al. (49) demonstrated a 14.5-fold increase in cellular uptake of mannose-coated vs uncoated NLCs, as determined by fluorescence microscopy and flow cytometry. Despite quantitative differences between studies, the data strongly support the conclusion that mannose functionalization significantly enhances NLCs internalization in macrophages.

Using a tumor-associated macrophage model, the treatment with NLC- β -Lap and NLC- β -Lap-MAN significantly increased IL-6 and TNF- α secretion, indicat-

ing a further pro-inflammatory M1-like polarization. However, no increase was observed for IL-8 secretion and a less marked enhancement in IL-1RA and IL-13 secretion was observed, further supporting this M1-like profile. Full confirmation of the macrophage phenotype switch will be performed in future studies using RT-qPCR and immunofluorescence.

Given the established role of macrophages in OS tumor metastasis (19-21), repolarizing them towards a pro-inflammatory phenotype or a M1-TAMs phenotype can be an excellent strategy to control OS. The administration of β -Lap loaded NLCs has the potential to enhance drug circulation time and tumor accumulation, facilitating TAMs phenotype modulation and creating an anti-tumoral environment (28). Additionally, the mannose functionalization of the NLCs significantly improve internalization by macrophages, promoting their repolarization toward a pro-inflammatory phenotype (M1-TAMs phenotype).

CONCLUSIONS

NLCs loaded with the anti-tumoral drug β -Lap and surface-functionalized with mannose were successfully developed for targeted drug delivery. AI tools, specifically ANNs, proved effective to accurately predict particle size, polydispersity index, and zeta potential of NLCs. However, drug loading predictions were less accurate, indicating the need for further model refinement or exploration of alternative loading strategies.

Mannose-functionalized NLCs exhibited enhanced macrophage uptake, crucial for targeted delivery to tumor-associated macrophages. Despite suboptimal drug loading, these systems stimulated the secretion of pro-inflammatory cytokines IL-6 and TNF- α , inducing macrophage polarization towards an anti-tumor phenotype. This suggests that even with lower drug concentrations, the targeted delivery and macrophage activation achieved with these NLCs hold significant therapeutic potential for osteosarcoma.

Future studies should be focused on optimizing drug loading efficiency through the screening of other raw materials or loading techniques. Additionally, *in vivo* studies are needed to evaluate the therapeutic efficacy of these mannose-functionalized NLCs in relevant OS models. The successful application of AI tools in predicting key NLC properties underscores their value in accelerating drug delivery system development.

REFERENCES

1. Kar E, Ammanamanchi A, Yousif M, Geetha SD, Schwartz K, Mishra AS, et al. From bimodal to unimodal: The transformed incidence of osteosarcoma in the United States. *J Bone Oncol* 2024;47:100613. DOI: 10.1016/j.jbo.2024.100613

2. Beird HC, Bielack SS, Flanagan AM, Gill J, Heymann D, Janeway KA, et al. Osteosarcoma. *Nat Rev Dis Primers* 2022;8(1):77. DOI: 10.1038/s41572-022-00409-y
3. Belayneh R, Fourman MS, Bhogal S, Weiss KR. Update on Osteosarcoma. *Curr Oncol Rep* 2021;23(6):71. DOI: 10.1007/s11912-021-01053-7
4. Mirabello L, Troisi RJ, Savage SA. Osteosarcoma incidence and survival rates from 1973 to 2004: data from the Surveillance, Epidemiology, and End Results Program. *Cancer* 2009;115(7):1531-43. DOI: 10.1002/cncr.24121
5. Cersosimo F, Lonardi S, Bernardini G, Telfer B, Mandelli GE, Santucci A, et al. Tumor-Associated Macrophages in Osteosarcoma: From Mechanisms to Therapy. *Int J Mol Sci* 2020;21(15):5207. DOI: 10.3390/ijms21155207
6. Picci P, Sangiorgi L, Caldora P, Benassi MS, Campanacci M. Histopatología del osteosarcoma. *Revista Española de Cirugía Osteoarticular* 1995;30(178):211-6.
7. Chen X, Bahrami A, Pappo A, Easton J, Dalton J, Hedlund E, et al.; St. Jude Children's Research Hospital–Washington University Pediatric Cancer Genome Project. Recurrent somatic structural variations contribute to tumorigenesis in pediatric osteosarcoma. *Cell Rep* 2014;7(1):104-12. DOI: 10.1016/j.celrep.2014.03.003
8. Behjati S, Tarpey PS, Haase K, Ye H, Young MD, Alexandrov LB, et al. Recurrent mutation of IGF signalling genes and distinct patterns of genomic rearrangement in osteosarcoma. *Nat Commun* 2017;8:15936. DOI: 10.1038/ncomms15936
9. Rothzerg E, Pfaff AL, Koks S. Innovative approaches for treatment of osteosarcoma. *Exp Biol Med (Maywood)* 2022;247(4):310-6. DOI: 10.1177/15353702211067718
10. Smith MA, Seibel NL, Altekruse SF, Ries LA, Melbert DL, O'Leary M, et al. Outcomes for children and adolescents with cancer: challenges for the twenty-first century. *J Clin Oncol* 2010;28(15):2625-34. DOI: 10.1200/JCO.2009.27.0421
11. Kathiresan N, Selvaraj C, Pandian S, Subbaraj GK, Alothaim AS, Safi SZ, et al. Proteomics and genomics insights on malignant osteosarcoma. *Adv Protein Chem Struct Biol* 2024;138:275-300. DOI: 10.1016/bs.apcsb.2023.06.001
12. Kansara M, Teng MW, Smyth MJ, Thomas DM. Translational biology of osteosarcoma. *Nat Rev Cancer* 2014;14(11):722-35. DOI: 10.1038/nrc3838
13. Klein MJ, Siegal GP. Osteosarcoma: anatomic and histologic variants. *Am J Clin Pathol* 2006;125(4):555-81. DOI: 10.1309/UC6K-QHLD-9LV2-KENN
14. Gao YM, Pei Y, Zhao FF, Wang L. Osteoclasts in Osteosarcoma: Mechanisms, Interactions, and Therapeutic Prospects. *Cancer Manag Res* 2023;15:1323-37. DOI: 10.2147/CMAR.S431213
15. Fernández-Tresguerres Hernández-Gil I, Alobera Gracia MA, del Canto Pingarrón, Blanco Jerez L. Bases fisiológicas de la regeneración ósea I. *Histología y fisiología del tejido óseo. Med Oral Patol Oral Cir Bucal* 2006;11:E47-51.
16. Wu C, Gong S, Duan Y, Deng C, Kallendrusch S, Berninghausen L, et al. A tumor microenvironment-based prognostic index for osteosarcoma. *J Biomed Sci* 2023;30(1):23. DOI: 10.1186/s12929-023-00917-3
17. Miwa S, Shirai T, Yamamoto N, Hayashi K, Takeuchi A, Igarashi K, et al. Current and Emerging Targets in Immunotherapy for Osteosarcoma. *J Oncol* 2019;2019:7035045. DOI: 10.1155/2019/7035045
18. Chim LK, Williams IL, Bashor CJ, Mikos AG. Tumor-associated macrophages induce inflammation and drug resistance in a mechanically tunable engineered model of osteosarcoma. *Biomaterials* 2023;296:122076. DOI: 10.1016/j.biomaterials.2023.122076
19. Champagne CM, Takebe J, Offenbacher S, Cooper LF. Macrophage cell lines produce osteoinductive signals that include bone morphogenetic protein-2. *Bone* 2002;30(1):26-31. DOI: 10.1016/s8756-3282(01)00638-x
20. Chen C, Xie L, Ren T, Huang Y, Xu J, Guo W. Immunotherapy for osteosarcoma: Fundamental mechanism, rationale, and recent breakthroughs. *Cancer Lett* 2021;500:1-10. DOI: 10.1016/j.canlet.2020.12.024
21. Wang Z, Wang Z, Li B, Wang S, Chen T, Ye Z. Innate Immune Cells: A Potential and Promising Cell Population for Treating Osteosarcoma. *Front Immunol* 2019;10:1114. DOI: 10.3389/fimmu.2019.01114
22. Buddingh EP, Kuijjer ML, Duim RA, Bürger H, Agelopoulos K, Myklebost O, et al. Tumor-infiltrating macrophages are associated with metastasis suppression in high-grade osteosarcoma: a rationale for treatment with macrophage activating agents. *Clin Cancer Res* 2011;17(8):2110-9. DOI: 10.1158/1078-0432.CCR-10-2047
23. Huang Q, Liang X, Ren T, Huang Y, Zhang H, Yu Y, et al. The role of tumor-associated macrophages in osteosarcoma progression - therapeutic implications. *Cell Oncol (Dordr)* 2021;44(3):525-39. DOI: 10.1007/s13402-021-00598-w
24. Tu B, Peng ZX, Fan QM, Du L, Yan W, Tang TT. Osteosarcoma cells promote the production of pro-tumor cytokines in mesenchymal stem cells by inhibiting their osteogenic differentiation through the TGF- β /Smad2/3 pathway. *Exp Cell Res* 2014;320(1):164-73. DOI: 10.1016/j.yexcr.2013.10.013
25. Anand N, Peh KH, Kolesar JM. Macrophage Repolarization as a Therapeutic Strategy for Osteosarcoma. *Int J Mol Sci* 2023;24(3):2858. DOI: 10.3390/ijms24032858
26. Meyers PA, Schwartz CL, Krailo MD, Healey JH, Bernstein ML, Betcher D, et al.; Children's Oncology Group. Osteosarcoma: the addition of muramyl tripeptide to chemotherapy improves overall survival--a report from the Children's Oncology Group. *J Clin Oncol* 2008;26(4):633-8. DOI: 10.1200/JCO.2008.14.009
27. Punzo F, Bellini G, Tortora C, Pinto DD, Argenziano M, Pota E, et al. Mifamurtide and TAM-like macrophages: effect on proliferation, migration and differentiation of osteosarcoma cells. *Oncotarget* 2020;11(7):687-98. DOI: 10.18632/oncotarget.27479
28. Ashique S, Faiyazuddin M, Afzal O, Gowri S, Hussain A, Mishra N, et al. Advanced nanoparticles, the hallmark of targeted drug delivery for osteosarcoma-an updated review. *J Drug Deliv Sci Technol* 2023;87:104753. DOI: 10.1016/j.jddst.2023.104753
29. Feng C, Jiang Y, Wang T, Tian D, Shen C, Wang Y, et al. Recent advances on nanostructured biomaterials in osteosarcoma treatment. *Coord Chem Rev* 2023;493:215315. DOI: 10.1016/j.ccr.2023.215315
30. Wang SY, Hu HZ, Qing XC, Zhang ZC, Shao ZW. Recent advances of drug delivery nanocarriers in osteosarcoma treatment. *J Cancer* 2020;11(1):69-82. DOI: 10.7150/jca.36588
31. Hori T, Kondo T, Lee H, Song CW, Park HJ. Hyperthermia enhances the effect of β -lapachone to cause γ H2AX formations and cell death in human osteosarcoma cells. *Int J Hyperthermia* 2011;27(1):53-62. DOI: 10.3109/02656736.2010.513361

32. Seoane S, Díaz-Rodríguez P, Sendon-Lago J, Gallego R, Pérez-Fernández R, Landin M. Administration of the optimized β-Lapachone-poloxamer-cyclodextrin ternary system induces apoptosis, DNA damage and reduces tumor growth in a human breast adenocarcinoma xenograft mouse model. *Eur J Pharm Biopharm* 2013;84(3):497-504. DOI: 10.1016/j.ejpb.2012.12.019
33. Silva VL, Al-Jamal WT. Exploiting the cancer niche: Tumor-associated macrophages and hypoxia as promising synergistic targets for nano-based therapy. *J Control Release* 2017;253:82-96. DOI: 10.1016/j.jconrel.2017.03.013
34. Tsai CF, Chen GW, Chen YC, Shen CK, Lu DY, Yang LY, et al. Regulatory Effects of Quercetin on M1/M2 Macrophage Polarization and Oxidative/Antioxidative Balance. *Nutrients* 2021;14(1):67. DOI: 10.3390/nu14010067
35. Covarrubias A, Byles V, Horng T. ROS sets the stage for macrophage differentiation. *Cell Res* 2013;23(8):984-5. DOI: 10.1038/cr.2013.88
36. Díaz-Rodríguez P, Landin M. Smart design of intratumoral thermosensitive β-lapachone hydrogels by Artificial Neural Networks. *Int J Pharm* 2012;433(1-2):112-8. DOI: 10.1016/j.ijpharm.2012.05.008
37. Aljabali AA, Obeid MA, Bashatwah RM, Serrano-Aroca Á, Mishra V, Mishra Y, et al. Nanomaterials and Their Impact on the Immune System. *Int J Mol Sci* 2023;24(3):2008. DOI: 10.3390/ijms24032008
38. Bordon G, Berenbaum F, Distler O, Luciani P. Harnessing the multifunctionality of lipid-based drug delivery systems for the local treatment of osteoarthritis. *Biomed Pharmacother* 2023;168:115819. DOI: 10.1016/j.biopha.2023.115819
39. Cummings RD. The mannose receptor ligands and the macrophage glycome. *Curr Opin Struct Biol* 2022;75:102394. DOI: 10.1016/j.sbi.2022
40. Fan S, Han H, Yan Z, Lu Y, He B, Zhang Q. Lipid-based nanoparticles for cancer immunotherapy. *Med Rev (2021) 2023*;3(3):230-69. DOI: 10.1515/mr-2023-0020
41. Martínez-Borrajo R, Rouco H, Virzi NF, Díaz-Rodríguez P, Landin M. Modulation of IFN-γ induced macrophage inflammatory responses via indomethacin-loaded NLCs for OA management. *Int J Pharm* 2024;666:124823. DOI: 10.1016/j.ijpharm.2024.124823
42. Colbourn EA, Roskilly SJ, Rowe RC, York P. Modelling formulations using gene expression programming--a comparative analysis with artificial neural networks. *Eur J Pharm Sci* 2011;44(3):366-74. DOI: 10.1016/j.ejps.2011.08.021
43. Landin M, Rowe RC, York P. Advantages of neurofuzzy logic against conventional experimental design and statistical analysis in studying and developing direct compression formulations. *Eur J Pharm Sci* 2009;38(4):325-31. DOI: 10.1016/j.ejps.2009.08.004
44. Martínez-Borrajo R, Díaz-Rodríguez P, Landin M. Rationalized design to explore the full potential of PLGA microspheres as drug delivery systems. *Drug Deliv* 2023;30(1):2219864. DOI: 10.1080/10717544.2023.2219864
45. Martínez-Borrajo R, Díaz-Rodríguez P, Landin M. Engineering mannose-functionalized nanostructured lipid carriers by sequential design using hybrid artificial intelligence tools. *Drug Deliv Transl Res* 2025;15(1):343-54. DOI: 10.1007/s13346-024-01603-z
46. Rouco H, Díaz-Rodríguez P, Rama-Molinos S, Remuñán-López C, Landin M. Delimiting the knowledge space and the design space of nanostructured lipid carriers through Artificial Intelligence tools. *Int J Pharm* 2018;553(1-2):522-30. DOI: 10.1016/j.ijpharm.2018.10.058
47. Rouco H, Díaz-Rodríguez P, Gaspar DP, Gonçalves LMD, Cuerva M, Remuñán-López C, et al. Rifabutin-Loaded Nanostructured Lipid Carriers as a Tool in Oral Anti-Mycobacterial Treatment of Crohn's Disease. *Nanomaterials (Basel)* 2020;10(11):2138. DOI: 10.3390/nano10112138
48. Vieira AC, Chaves LL, Pinheiro M, Ferreira D, Sarmiento B, Reis S. Design and statistical modeling of mannose-decorated dapson-containing nanoparticles as a strategy of targeting intestinal M-cells. *Int J Nanomedicine* 2016;11:2601-17. DOI: 10.2147/IJN.S104908
49. Vieira AC, Magalhães J, Rocha S, Cardoso MS, Santos SG, Borges M, et al. Targeted macrophages delivery of rifampicin-loaded lipid nanoparticles to improve tuberculosis treatment. *Nanomedicine (Lond)* 2017;12(24):2721-2736. DOI: 10.2217/nnm-2017-0248
50. Oishi Y, Manabe I. Macrophages in inflammation, repair and regeneration. *Int Immunol* 2018;30(11):511-28. DOI: 10.1093/intimm/dxy054
51. Schlundt C, Fischer H, Bucher CH, Rendenbach C, Duda GN, Schmidt-Bleek K. The multifaceted roles of macrophages in bone regeneration: A story of polarization, activation and time. *Acta Biomater* 2021;133:46-57. DOI: 10.1016/j.actbio.2021.04.052
52. Dias RB, de Araújo TBS, de Freitas RD, Rodrigues ACBDC, Sousa LP, Sales CBS, et al. β-Lapachone and its iodine derivatives cause cell cycle arrest at G2/M phase and reactive oxygen species-mediated apoptosis in human oral squamous cell carcinoma cells. *Free Radic Biol Med* 2018;126:87-100. DOI: 10.1016/j.freeradbiomed.2018.07.022
53. de Andrade JKF, da Silva Góes AJ, Barbosa VX, de Lima Silva MS, Matos Donato MA, et al. Anticancer activity of β-Lapachone derivatives on human leukemic cell lines. *Chem Biol Interact* 2022;365:110057. DOI: 10.1016/j.cbi.2022.110057
54. Li X, Jia X, Niu H. Nanostructured lipid carriers co-delivering lapachone and doxorubicin for overcoming multidrug resistance in breast cancer therapy. *Int J Nanomedicine* 2018;13:4107-19. DOI: 10.2147/IJN.S163929
55. Mytar B, Woloszyn M, Macura-Bieguna A, Hajto B, Ruggiero I, Piekarska B, et al. Involvement of pattern recognition receptors in the induction of cytokines and reactive oxygen intermediates production by human monocytes/macrophages stimulated with tumor cells. *Anticancer Res* 2004;24(4):2287-93.
56. Wollman J, Wanniarachchi K, Pradhan B, Huang L, Kerkvliet JG, Hoppe AD, et al. Mannose receptor (MRC1) mediates uptake of dextran by bone marrow-derived macrophages. *Mol Biol Cell* 2024;35(12):ar153. DOI: 10.1091/mbc.E24-08-0355
57. Ahalwat S, Bhatt DC, Rohilla S, Jogpal V, Sharma K, Virmani T, et al. Mannose-Functionalized Isoniazid-Loaded Nanostructured Lipid Carriers for Pulmonary Delivery: In Vitro Prospects and In Vivo Therapeutic Efficacy Assessment. *Pharmaceuticals (Basel)* 2023;16(8):1108. DOI: 10.3390/ph16081108